ORIGINAL RESEARCH

Tandem Mass Tag-Based Proteomic Analysis of Normal and Degenerated Human Intervertebral Discs

Yang Fu*, Xiao-Qin Huang*, Hang-Bo Qu, Yan Zhi Ge, Xuan-Liang Ru

Department of Orthopedics, Zhejiang Hospital, Hangzhou, Zhejiang Province, People's Republic of China

*These authors contributed equally to this work

Correspondence: Xuan-Liang Ru, Department of Orthopedics, Zhejiang Hospital, No. 1229 Gudun Road, Hangzhou, Zhejiang Province, 310013, People's Republic of China, Tel +86-133-3612-4875, Email zjyyrxl@qq.com

Background: Intervertebral disc degeneration (IVDD) is the main cause of low back pain (LBP), but the specific regulatory factors, pathways and specific molecular mechanisms remain unclear.

Methods: We identified and quantitatively analyzed Pfirrmann Grade II (n=3) and Pfirrmann Grade IV (n=3) pulposus samples via MRI. The differential abundance of proteins in the samples was determined and quantitatively analyzed by relative and absolute quantitative analysis of the isotope marker levels combined with the liquid chromatography–tandem mass spectrometry (LC–MSMS/MS).

Results: A total of 70 proteins (30 significantly increased proteins (> 1.2-fold change) and 40 significantly decreased proteins (< 0.8-fold change)) showed different levels among the groups. Kyoto Encyclopedia of Genes and Genomes and Gene Ontology (GO) enrichment analyses and Western blot analysis showed that CYCS, RAC1, and PSMD14 may play important roles in IVDD and that Epstein–Barr virus infection, viral myocarditis, colorectal cancer, nonalcoholic fatty liver disease (NAFLD) and amyotrophic lateral sclerosis (ALS) are the main pathways involved in IVDD.

Conclusion: CYCS, RAC1 and PSMD14 may play important roles in IVDD, and Epstein–Barr virus infection, viral myocarditis, colorectal cancer, NAFLD and ALS may be the main pathways involved in IVDD.

Keywords: TMT, LC–MS/MS, proteomics, low back pain, nucleus pulposus

Instruction

Low back pain (LBP) is an important disease that endangers the lives of people worldwide and has an incidence greater than 70%,[1] but its pathogenic mechanism remains unclear. Lumbar disc degeneration is an important factor leading to LBP, especially in middle-aged and elderly patients.[2] The mechanism underlying the occurrence and development of lumbar intervertebral disc degeneration (IVDD) is complex, and age is the main risk factor.[3] The currently available drugs can alleviate only the clinical manifestations of LBP but cannot eliminate the underlying problem. Studying aging-related degenerative IVDD is key to identifying a new strategy for preventing and treating IVDD.[4]

IVDD is initiated in the nucleus pulposus (NP), which is located at the center of a disc.[5] Degenerative lesions in the lumbar spine generally have no obvious clinical manifestations but are accompanied by loss of water and proteoglycans. In general, degenerated discs become fibrotic and cannot absorb shock. Moreover, age-related IVDD is attributed to rapid changes in the anatomic and pathophysiological characteristics after birth.[6] According to magnetic resonance imaging (MRI), lumbar disc degeneration can be divided into five grades according to the Pfirrmann grade: Grade I indicates a normal degree of degeneration, Grade II is considered to indicate mild degeneration, Grade III is thought to indicate moderate degeneration, and Grades IV and V denote severe degeneration.[7,8] The aging of organisms and the resulting pathophysiological changes can be detected at the protein level. However, the previous studies on age-related IVDD have been limited to a few proteins and

pathways.[9] At present, experiments are commonly used, but their results do not directly reflect the severity of IVDD.[10] In general, few studies have performed a comprehensive evaluation of the protein profile of lumbar intervertebral discs, especially human NP specimens.[11] Proteomics is a cross-disciplinary field in which the composition, function and interrelation of proteins are studied in their entirety. Differential proteome analysis is a good method for evaluating the protein levels in samples because it enables protein screening and identification of the whole protein network in samples.[12] With the continuous development of proteomics technology, stable isotope labeling, especially tandem mass tag (TMT) labeling, combined with mass spectrometry (MS) has become the main method used for protein quantitative analysis.[13] This method has tremendously facilitated the study of the mechanisms linked to degenerate diseases. Compared with genomics and transcriptomics, quantitative proteomics is an ideal tool for obtaining insights into overall proteome differences. Potential biomarkers and mechanisms can be elucidated by proteomics using isobaric tags (TMT or iTRAQ) and bioinformatics analysis. Therefore, this study used differential proteomics technology to analyze the proteins in the intervertebral disc tissues of people of different ages with the aim of establishing a foundation for studying the mechanism underlying IVDD.

In the present study, we collected NP samples from patients with different tumor grades on MRI and used TMT labeling combined with liquid chromatography (LC)-tandem MS (MS/MS) to detect differentially expressed proteins (DEPs). This study used TMT-based proteomic technology to screen DEPs closely related to IVDD and combined this information with the results from bioinformatics methods to identify important proteins and their corresponding signal transduction pathways closely related to IVDD.

Materials and Methods

Participants and Sample Collection

NP specimens of human lumbar L4/5 intervertebral discs of Pfirrmann Grade II were collected to establish the mild group (n=3); NP specimens of human lumbar L4/5 intervertebral discs of Pfirrmann Grade IV comprised the severe group (n=3). All patients were diagnosed with single-level lumbar disc herniation (Supplemental Material 1). Patients with spinal trauma, tumors, or infections; a history of diabetes; obesity; or an autoimmune disease were excluded. Their clinical diagnosis was confirmed by imaging and physical examination by two spine surgeons and a radiologist. The NPs were separated using a stereomicroscope and then rinsed with sterile saline to remove all blood stains and impurities on the tissue surface; the samples were then preserved with liquid nitrogen.

Filter-Aided Sample Preparation (FASP)

Two hundred micrograms of protein was added to 30 μL of SDT buffer (4% sodium dodecyl sulfate, 100 mmol of DTT, and 150 mmol of Tris-HCl, pH 8.0). Detergents, DTT and other small-molecule components were used as uric acid buffers (8 M urea, 150 mM Tris-HCl, pH 8.5). To prevent the condensation of cysteine residues, 100 μL of iodoacetamide (100 mM IAA in uric acid buffer) was added, and the mixture was incubated in the dark for 30 min. The filter was washed three times with 100 μL of UA buffer and then with 100 μL of 0.1 M TEAB buffer. The peptides were then digested with 4 μg of trypsin (Promega) in 40 μL of 0.1 M TEAB buffer at 37 °C and filtered. Using an extinction factor of 1.1 g/L, the content of tryptophan and tyrosine in polypeptides in vertebrate proteins was estimated by UV spectroscopy at 280 nm.

TMT Labeling

According to the manufacturer's instructions (Thermo Fisher Science), 100 μg of polypeptide mixture was labeled with TMT reagent.

Peptide Fractionation with Reversed-Phase (RP) Chromatography

The TMT-labeled peptides were analyzed by chromatography with an Agilent 1260 infinity II HPLC. An XBridge Peptide BEHC18 chromatographic column (130 μm, 5 μm, 4.6 mm×100 mm) was loaded with buffer

1314

Journal of Pain Research 2024:17

A (10 mM HCOONH$_4$ and 5% ACN, pH 10.0). The polypeptides were eluted at a rate of 1 mL/min with the following program: 0 to 7% buffer B (10 mM HCOONH4, 85% ACN, pH 10.0) for 5 min, buffer B for 7 to 40 min, buffer B for 45 to 50 min, and 50 to 65 min. The time interval of 5 to 50 min was monitored by ultraviolet (UV) tracking at 214 nm, and samples were collected during this period. The collected components were concentrated into 10 components and dried by vacuum centrifugation at 45°C.

Mass Spectrometry Analysis
EASY-nLC
The components were determined by nano-liquid chromatography–mass spectrometry. The mixture of the peptides was packed in buffer A (0.1% formic acid) in a C18 inversion analyzer (Thermo Fisher Science, Nano Viper, Accept PepMap RSLC 50 μm × 15 cm, P/N164943) and separated using a linear gradient of buffer B (80% acetonitrile and 0.1% formic acid) at 300 nl/min.

The following 1.5-h gradient was utilized: 6% buffer B for 5 min, 6–28% buffer B for 63 min, 28–38% buffer B for 10 min, 38–100% buffer B for 7 min, and 100% buffer B for 5 min.

LC–MS/MS Analysis
Q-Exactive MS (Thermo Fisher Science) and EASY-nLC (Thermo Fisher Science) were used for 90 min. The mass spectrum depends on positive charges. In this study, the first 10 different MS techniques were used to analyze the largest precursors in the existing HCD particle spectra (350–1800 m/z). On this basis, the detection of 70,000 m/z 200 3e6 with a maximum transmittance (50 ms) was achieved. For the m/z200 HCD band, the scanning power of MS2 had a resolution of 17,500, 2e5 was the target of AGC, and the maximum IT value was 45 ms. On this basis, we selected ions with 2–6 charges and set the minimum amount of fragmented materials to 2e3. The selected ions were dynamically removed after 30s. The standard collision energy was 30 electronvolts.

Data Analysis
The MASCOT engine was built into Proteome Discoverer 2.2 (Matrix Science, London, UK; 2.6), which processes raw MS/MS documents and retrieves them from UniProt-Homo_sapiens.fasta. The search parameters included trypsin-generated peptides and allowed a maximum of 2 missed cleavages. A precursor mass of 10 ppm and an MS2 fragment of 0.05 Da were specified. The amino acid (C) sequence was set as a fixed modification in addition to the TMT tag. The variable modifications were (M)oxidation and acetylation (N-protein). A reverse database search strategy was used to increase the detection rate of peptides and proteins by 1% (fold variation of 1.2, p value determined by Student's t-test).

Bioinformatics Analysis
Gene Ontology (GO) Annotation
First, all protein sequences were compared with UniProt-GOA data, and only the top 10 sequences with E value "=1e-3" were compared. Second, the GO term in the bit-Score sequence in Blast2 GO was selected. Next, annotation from GO to protein was performed by the Blast2 GO command line. After completing the basic annotation, InterProScan was used to search the EBI database for motifs and add information on motif function to the protein, thus improving the annotation. Then, ANNEX was used to annotate and link the GO terms. Fisher's exact test was used to enrich the GO terms by comparing the DEPs and the total amount of proteins with the GO terms.

KEGG Pathway Annotation
Through an analysis of KEGG data, the related metabolic pathways were identified. The enrichment of different metabolic pathways was analyzed by Fisher's exact test.

Western Blot
Total protein was extracted from disc samples by RIPA lysis buffer and boiled in sample buffer in a water bath for 10 min. A total of 30 μg of protein sample was then separated via 10% SDS–PAGE for 2 h, after which the proteins were

transferred to a polyvinylidene difluoride membrane. The membrane was blocked in 5% nonfat milk at room temperature for 1 h and then incubated with primary antibodies against GAPDH (1:1000; Cell Signaling Technology, CST), Rac1 (1:1000; CST), CYCS (1:1000; CST), PSMD14 (1:1000; Abcam), COPS4 (1:1000; CST), and tubulin (1:1000; CST) overnight at 4°C. The following day, the membrane was washed three times with Tris-buffered saline and Tween and then incubated with goat anti-rabbit (1:5000, Abways) secondary antibodies at room temperature for 1 h. The antigen–antibody complexes were washed again and visualized via enhanced chemiluminescence.

Statistical Analysis

The two-tailed Mann–Whitney and Fisher's exact tests were performed with SigmaPlot software. The values are expressed as the means ± SEMs. P < 0.05 was considered to indicate statistical significance. The P value was not adjusted by the false discovery rate.

Results
SDS–PAGE

Proteins in the Grade II and Grade IV NP samples were separated by SDS–PAGE. Among the 6 samples, all the proteins between 15 and 220 kDa in length were efficiently isolated without protein degradation, indicating that the protein content in the samples was sufficient for future experiments.

LC–MS/MS Spectrum Analysis and Identification of DEPs

Liquid chromatography–mass spectrometry (LC–MS/MS) has become an important technique used in NP research. We found 2042 NP proteins, and 70 NP proteins were found by screening via LC–MS (Table 1 and Supplemental Material 2). The levels of 30 NP proteins increased, whereas the levels of 40 NP proteins decreased (Figure 1). A cluster study of the DEPs revealed

Table 1 DEPs Between NP Samples from Mild and Severe Group

Change	Protein Accession Number	Protein Description	Gene name
Increased	P05496	ATP synthase F(0) complex subunit C1, mitochondrial OS=Homo sapiens OX=9606 GN=ATP5MC1 PE=1 SV=2	ATP5MC1
Increased	Q6P528	ASPN protein OS=Homo sapiens OX=9606 GN=ASPN PE=2 SV=1	ASPN
Increased	A0A5C2FYV4	IGL c2198_light_IGLV2-8_IGLJ2 (Fragment) OS=Homo sapiens OX=9606 PE=2 SV=1	/
Increased	A0A5C2GA04	IGH + IGL c22_light_IGLV3-25_IGLJ1 (Fragment) OS=Homo sapiens OX=9606 PE=2 SV=1	/
Increased	A0A5C2G087	IGL c1365_light_IGKV1-17_IGKJ4 (Fragment) OS=Homo sapiens OX=9606 PE=2 SV=1	/
Increased	A0A5C2GFF7	IG c500_heavy_IGHV3-23_IGHD6-19_IGHJ4 (Fragment) OS=Homo sapiens OX=9606 PE=2 SV=1	/
Increased	A0A1B0GVN9	Uroporphyrinogen decarboxylase OS=Homo sapiens OX=9606 GN=UROD PE=1 SV=1	UROD
Increased	Q7Z351	Uncharacterized protein DKFZp686N02209 OS=Homo sapiens OX=9606 GN=DKFZp686N02209 PE=2 SV=1	DKFZ
Increased	P54851	Epithelial membrane protein 2 OS=Homo sapiens OX=9606 GN=EMP2 PE=1 SV=1	EMP2
Increased	A0A5C2GJY0	IG c758_light_IGKV3-20_IGKJ3 (Fragment) OS=Homo sapiens OX=9606 PE=2 SV=1	/
Increased	Q08722	Leukocyte surface antigen CD47 OS=Homo sapiens OX=9606 GN=CD47 PE=1 SV=1	CD47
Increased	A0A5C2GXC2	IG c1247_heavy_IGHV1-69_IGHD1-1_IGHJ6 (Fragment) OS=Homo sapiens OX=9606 PE=2 SV=1	/
Increased	A0A024R1U4	RAB5C, member RAS oncogene family, isoform CRA_a OS=Homo sapiens OX=9606 GN=RAB5C PE=4 SV=1	RAB5C
Increased	A0A5C2GAR1	IGH + IGL c172_heavy_IGHV3-23_IGHD2-21_IGHJ4 (Fragment) OS=Homo sapiens OX=9606 PE=2 SV=1	/
Increased	D6RJI3	Fibrillin-2 OS=Homo sapiens OX=9606 GN=FBN2 PE=1 SV=1	FBN2
Increased	O43263	RNA editing deaminase 1 OS=Homo sapiens OX=9606 GN=hRED1 PE=4 SV=1	hRED1
Increased	A8K5T0	cDNA FLJ75416, highly similar to Homo sapiens complement factor H (CFH), mRNA OS=Homo sapiens OX=9606 PE=2 SV=1	/
Increased	Q9HBA0	Transient receptor potential cation channel subfamily V member 4 OS=Homo sapiens OX=9606 GN=TRPV4 PE=1 SV=2	TRPV4
Increased	P54707	Potassium-transporting ATPase alpha chain 2 OS=Homo sapiens OX=9606 GN=ATP12A PE=1 SV=3	ATP12A
Increased	A0A2U8J8Z6	Ig heavy chain variable region (Fragment) OS=Homo sapiens OX=9606 GN=IgH PE=2 SV=1	IgH
Increased	C9JFR7	Cytochrome c (Fragment) OS=Homo sapiens OX=9606 GN=CYCS PE=1 SV=1	CYCS
Increased	B2RD19	cDNA, FLJ96419, highly similar to Homo sapiens fructosamine-3-kinase-related protein (FN3KRP), mRNA OS=Homo sapiens OX=9606 PE=2 SV=1	/

(Continued)

Table 1 (Continued).

| Change	Protein Accession Number	Protein Description	Gene name
Increased	A0A5C2GED2	IGH + IGL c407_heavy_IGHV1-69_IGHD6-13_IGHJ6 (Fragment) OS=Homo sapiens OX=9606 PE=2 SV=1	/
Increased	P50502	Hsc70-interacting protein OS=Homo sapiens OX=9606 GN=ST13 PE=1 SV=2	ST13
Increased	B2R7L2	Annexin OS=Homo sapiens OX=9606 PE=2 SV=1	/
Increased	A4D2P0	Ras-related C3 botulinum toxin substrate 1 (Rho family, small GTP binding protein Rac1) OS=Homo sapiens OX=9606 GN=RAC1 PE=2 SV=1	RAC1
Increased	O00487	26S proteasome non-ATPase regulatory subunit 14 OS=Homo sapiens OX=9606 GN=PSMD14 PE=1 SV=1	PSMD14
Increased	G3V4C1	Heterogeneous nuclear ribonucleoproteins C1/C2 OS=Homo sapiens OX=9606 GN=HNRNPC PE=1 SV=1	HNRNPC
Increased	P48163	NADP-dependent malic enzyme OS=Homo sapiens OX=9606 GN=ME1 PE=1 SV=1	ME1
Increased	Q71UI9	Histone H2A.V OS=Homo sapiens OX=9606 GN=H2AFV PE=1 SV=3	H2AFV
Decreased	D6RFN0	COP9 signalosome complex subunit 4 OS=Homo sapiens OX=9606 GN=COPS4 PE=1 SV=1	COPS4
Decreased	P60827	Complement C1q tumor necrosis factor-related protein 8 OS=Homo sapiens OX=9606 GN=C1QTNF8 PE=1 SV=2	C1QTNF8
Decreased	Q6PKX1	Myocilin (Fragment) OS=Homo sapiens OX=9606 GN=MYOC PE=4 SV=1	MYOC
Decreased	A0A172Q3A0	Fibroblast activation protein (Fragment) OS=Homo sapiens OX=9606 PE=2 SV=1	/
Decreased	A0A5C2GT30	IG c701_heavy_IGHV3-33_IGHD5-24_IGHJ2 (Fragment) OS=Homo sapiens OX=9606 PE=2 SV=1	/
Decreased	G3V357	Ribonuclease pancreatic OS=Homo sapiens OX=9606 GN=RNASE1 PE=1 SV=1	RNASE1
Decreased	Q9NR99	Matrix-remodeling-associated protein 5 OS=Homo sapiens OX=9606 GN=MXRA5 PE=1 SV=3	MXRA5
Decreased	Q14324	Myosin-binding protein C, fast-type OS=Homo sapiens OX=9606 GN=MYBPC2 PE=1 SV=2	MYBPC2
Decreased	B4E3L5	cDNA FLJ54656, highly similar to Aryl hydrocarbon receptor nuclear translocator OS=Homo sapiens OX=9606 PE=2 SV=1	/
Decreased	E9PP21	Cysteine and glycine-rich protein 1 OS=Homo sapiens OX=9606 GN=CSRP1 PE=1 SV=1	CSRP1
Decreased	A0A5C2GMH6	IG c556_heavy_IGHV1-46_IGHD3-22_IGHJ6 (Fragment) OS=Homo sapiens OX=9606 PE=2 SV=1	/
Decreased	A0A5C2FX56	IGL c175_light_IGKV3-11_IGKJ4 (Fragment) OS=Homo sapiens OX=9606 PE=2 SV=1	/
Decreased	A0A494C0B4	UV excision repair protein RAD23 homolog A OS=Homo sapiens OX=9606 GN=RAD23A PE=1 SV=1	RAD23A
Decreased	E9M263	Hemoglobin beta chain (Fragment) OS=Homo sapiens OX=9606 GN=HBB PE=3 SV=1	HBB
Decreased	A0A0G2JLB3	Glucosylceramidase OS=Homo sapiens OX=9606 GN=GBA PE=1 SV=1	GBA
Decreased	Q9NQ79	Cartilage acidic protein 1 OS=Homo sapiens OX=9606 GN=CRTAC1 PE=1 SV=2	CRTAC1
Decreased	A0A5C2GHJ7	IG c1102_heavy_IGHV3-74_IGHD3-22_IGHJ4 (Fragment) OS=Homo sapiens OX=9606 PE=2 SV=1	/
Decreased	P35908	Keratin, type II cytoskeletal 2 epidermal OS=Homo sapiens OX=9606 GN=KRT2 PE=1 SV=2	KRT2
Decreased	A8K7Q1	cDNA FLJ77770, highly similar to Homo sapiens nucleobindin 1 (NUCB1), mRNA OS=Homo sapiens OX=9606 PE=2 SV=1	/
Decreased	P13645	Keratin, type I cytoskeletal 10 OS=Homo sapiens OX=9606 GN=KRT10 PE=1 SV=6	KRT10
Decreased	Q8IUX7	Adipocyte enhancer-binding protein 1 OS=Homo sapiens OX=9606 GN=AEBP1 PE=1 SV=1	AEBP1
Decreased	A0A5C2GF02	IGH + IGL c459_heavy_IGHV3-23_IGHD6-19_IGHJ4 (Fragment) OS=Homo sapiens OX=9606 PE=2 SV=1	/
Decreased	A0A024R6P0	Serpin peptidase inhibitor, clade A (Alpha-1 antiproteinase, antitrypsin), member 3, isoform CRA_c OS=Homo sapiens OX=9606 GN=SERPINA3 PE=3 SV=1	/
Decreased	H6VRF8	Keratin 1 OS=Homo sapiens OX=9606 GN=KRT1 PE=3 SV=1	KRT1
Decreased	P45378	Troponin T, fast skeletal muscle OS=Homo sapiens OX=9606 GN=TNNT3 PE=1 SV=3	TNNT3
Decreased	Q13438	Protein OS-9 OS=Homo sapiens OX=9606 GN=OS9 PE=1 SV=1	OS9
Decreased	P35527	Keratin, type I cytoskeletal 9 OS=Homo sapiens OX=9606 GN=KRT9 PE=1 SV=3	KRT9
Decreased	Q9UKX2	Myosin-2 OS=Homo sapiens OX=9606 GN=MYH2 PE=1 SV=1	MYH2
Decreased	P58215	Lysyl oxidase homolog 3 OS=Homo sapiens OX=9606 GN=LOXL3 PE=1 SV=1	LOXL3
Decreased	A0A024R462	Fibronectin 1, isoform CRA_n OS=Homo sapiens OX=9606 GN=FN1 PE=4 SV=1	FN1
Decreased	Q6IAT9	Proteasome subunit beta OS=Homo sapiens OX=9606 GN=PSMB6 PE=2 SV=1	PSMB6
Decreased	P13647	Keratin, type II cytoskeletal 5 OS=Homo sapiens OX=9606 GN=KRT5 PE=1 SV=3	KRT5
Decreased	Q53R15	Uncharacterized protein MYL1 (Fragment) OS=Homo sapiens OX=9606 GN=MYL1 PE=4 SV=1	MYL1
Decreased	A0A5C2GVP3	IG c617_heavy_IGHV3-7_IGHD6-19_IGHJ3 (Fragment) OS=Homo sapiens OX=9606 PE=2 SV=1	/
Decreased	Q99592	Zinc finger and BTB domain-containing protein 18 OS=Homo sapiens OX=9606 GN=ZBTB18 PE=1 SV=1	ZBTB18
Decreased	B7Z7F6	cDNA FLJ51136, weakly similar to Aquaporin-7 OS=Homo sapiens OX=9606 PE=2 SV=1	/
Decreased	P02585	Troponin C, skeletal muscle OS=Homo sapiens OX=9606 GN=TNNC2 PE=1 SV=2	TNNC2
Decreased	A0A5C2G830	IGH c558_heavy__IGHV3-43_IGHD3-10_IGHJ1 (Fragment) OS=Homo sapiens OX=9606 PE=2 SV=1	/
Decreased	H3BPK4	Myosin regulatory light chain 2, skeletal muscle isoform (Fragment) OS=Homo sapiens OX=9606 GN=MYLPF PE=1 SV=1	MYLPF
Decreased	O75976	Carboxypeptidase D OS=Homo sapiens OX=9606 GN=CPD PE=1 SV=2	CPD
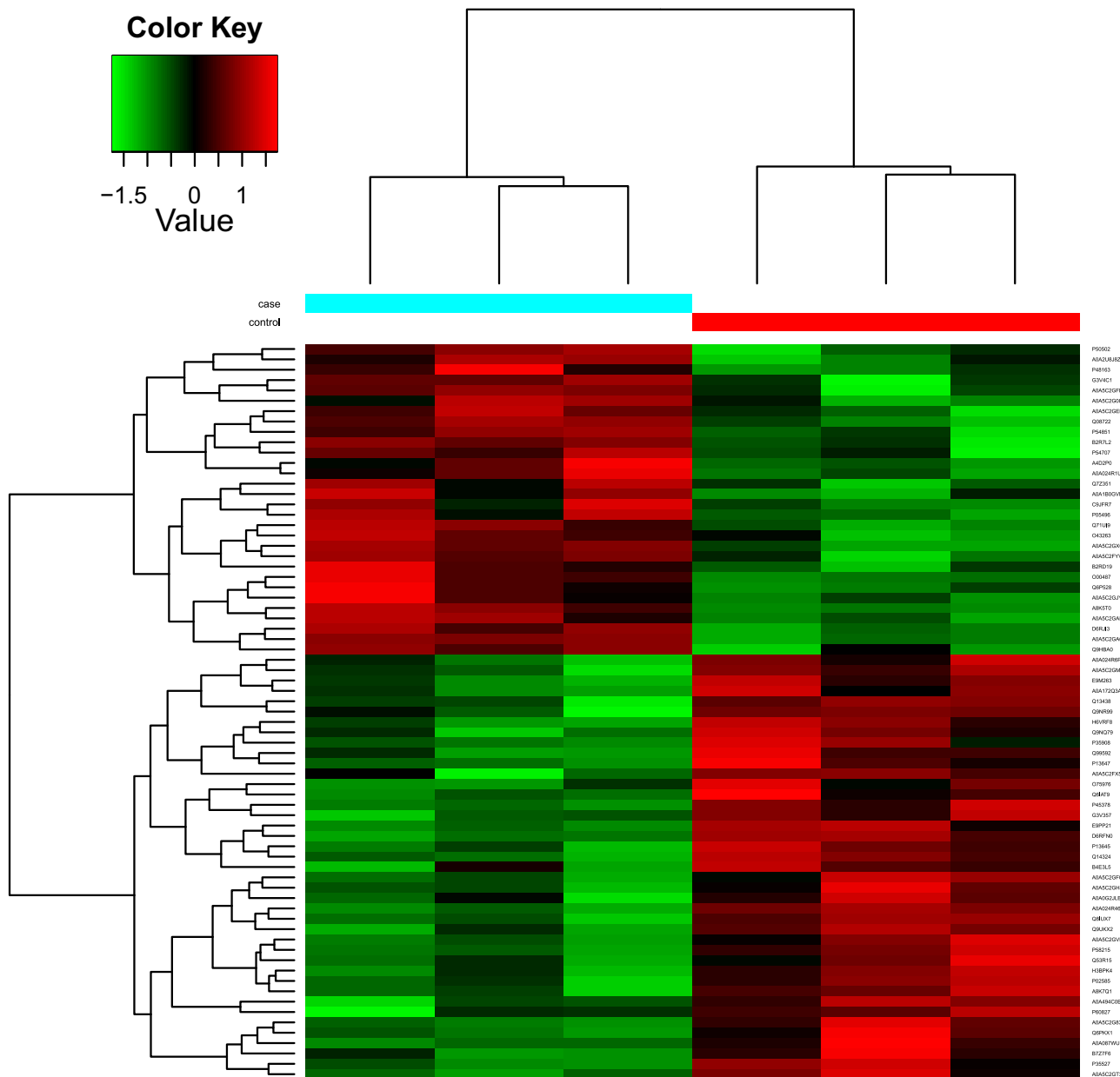
Figure 1 Heatmap of DEPs. Each row represents a protein, each column represents a sample/repeat, and each color represents a different expression level (log10 for quantification and median correction). The P value was not adjusted for the false discovery rate.

significant differences in the protein expression profiles between patients with relatively less severe IVDD and those with more severe IVDD. The decline and expansion of the critical DEP target network are shown in Figures 2 and 3.
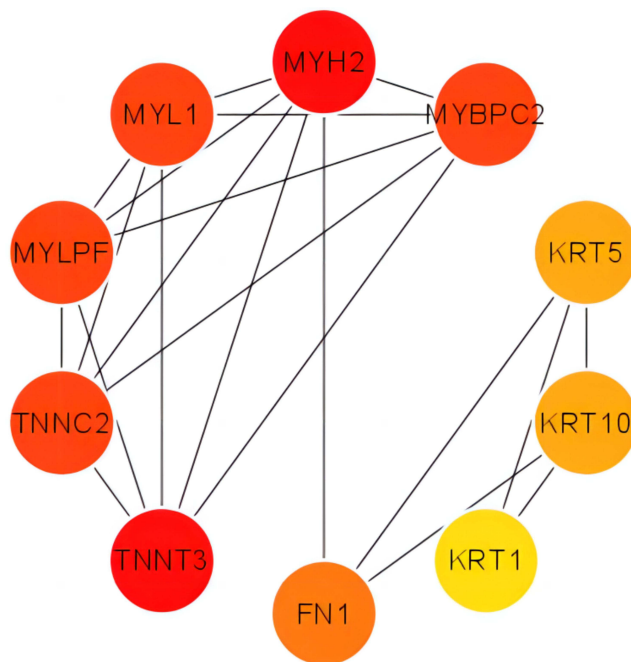
GO Annotation Enrichment Analysis

GO analysis has important application value in studies of cell composition, function and life activities. The GO functional annotations represent the numbers of these three types of DEPs. Through an enrichment analysis of GO functions, we obtained several GO functions related to the abovementioned DEPs (Supplemental Material 3). DEPs affect the physiological activities of cells through synergistic effects, and studying the underlying metabolic pathway will improve our understanding of their physiological functions. On this basis, we identified pathways associated with the accumulated DEPs and identified the most important biochemical synthesis pathway and signal transduction pathway. According to the results from the GO functional annotation of biological processes, the largest proportion of DEPs (21 proteins) were related to the term "cellular process", and
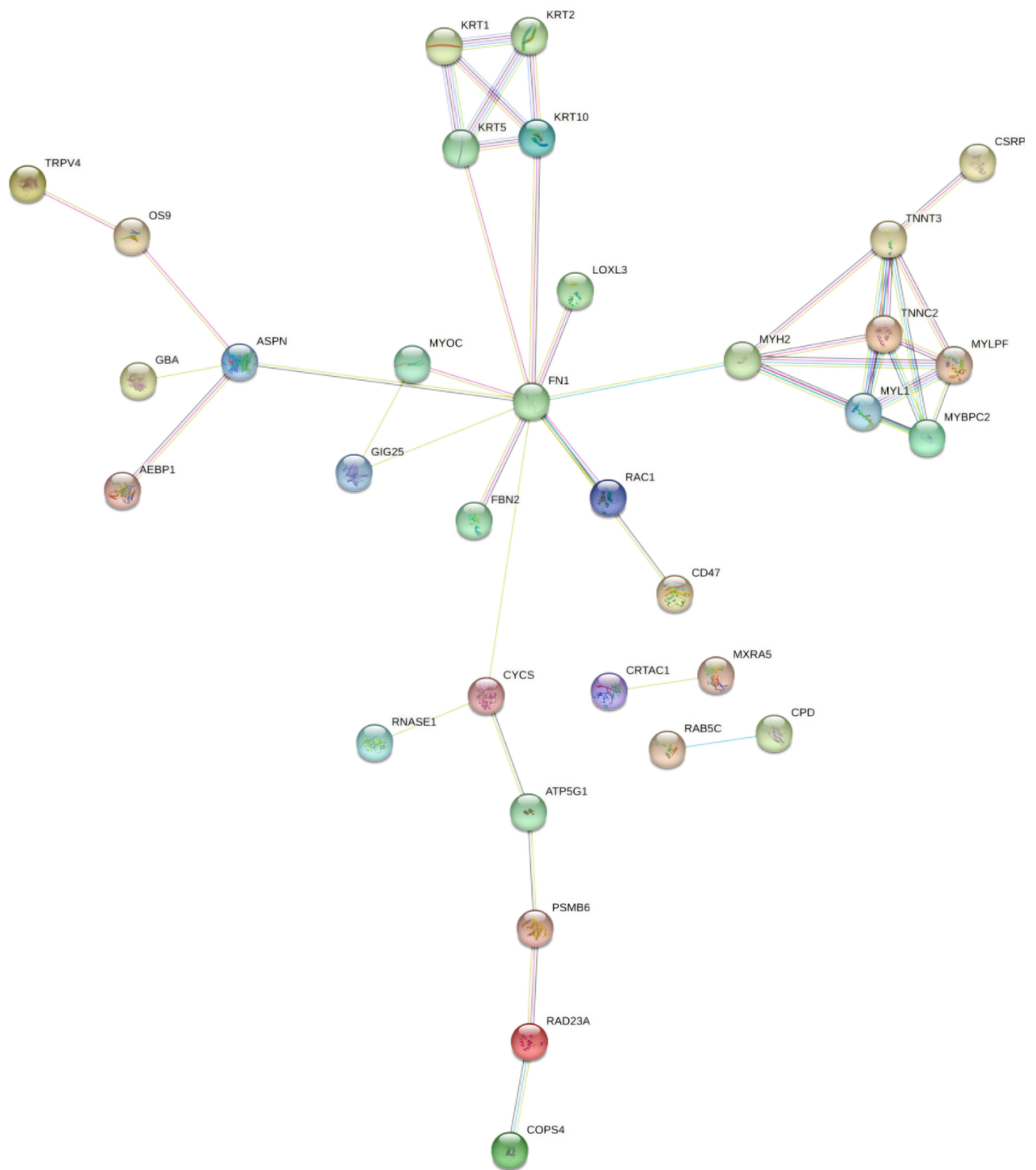
Figure 2 Key target network of the downregulated DEPs in the severe and mild groups. The line represents a protein interaction recorded or predicted by STRING, and each box represents a key protein recorded by Cytoscape.

the three top proteins were RNASE1, MYBPCF and IGHJ6. Among the cellular component terms, the highest percentage of proteins were related to the "cellular anatomical entity" (n = 29), and COPS4, C1QTNF8 and MYOC were found at the highest levels. From the perspective of molecular biology, the largest proportion of proteins was related to "binding" (n = 24), and MYOC, RNASE1 and MYBPCF were responsible for the greatest effect (Figure 4).

**Figure 3** Key network of upregulated DEPs in the severe and mild groups.
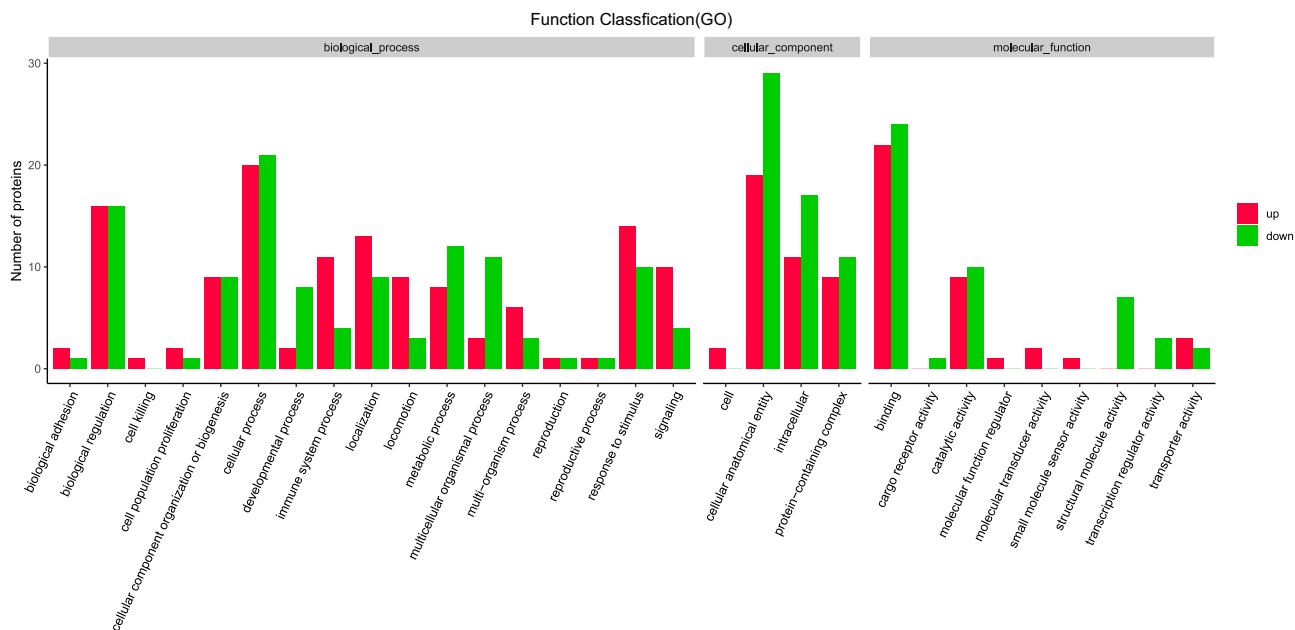
Figure 4 GO annotations for functional classification.

A functional enrichment analysis of the GO data found that increases in the number of DEPs were related to the regulation of carboxylase activity, nitric oxide biosynthesis and the production of IL-6, whereas decreases in the number of DEPs were related to terms describing the function of the DEPs, which included intermediate filament and keratinization (Figure 5).

KEGG Pathway Annotation and Enrichment

KOBAS online analysis software was used to identify the role of DEPs and to perform a KEGG analysis of signal transduction pathways. Among the candidate pathways identified, the five most relevant KEGG signaling
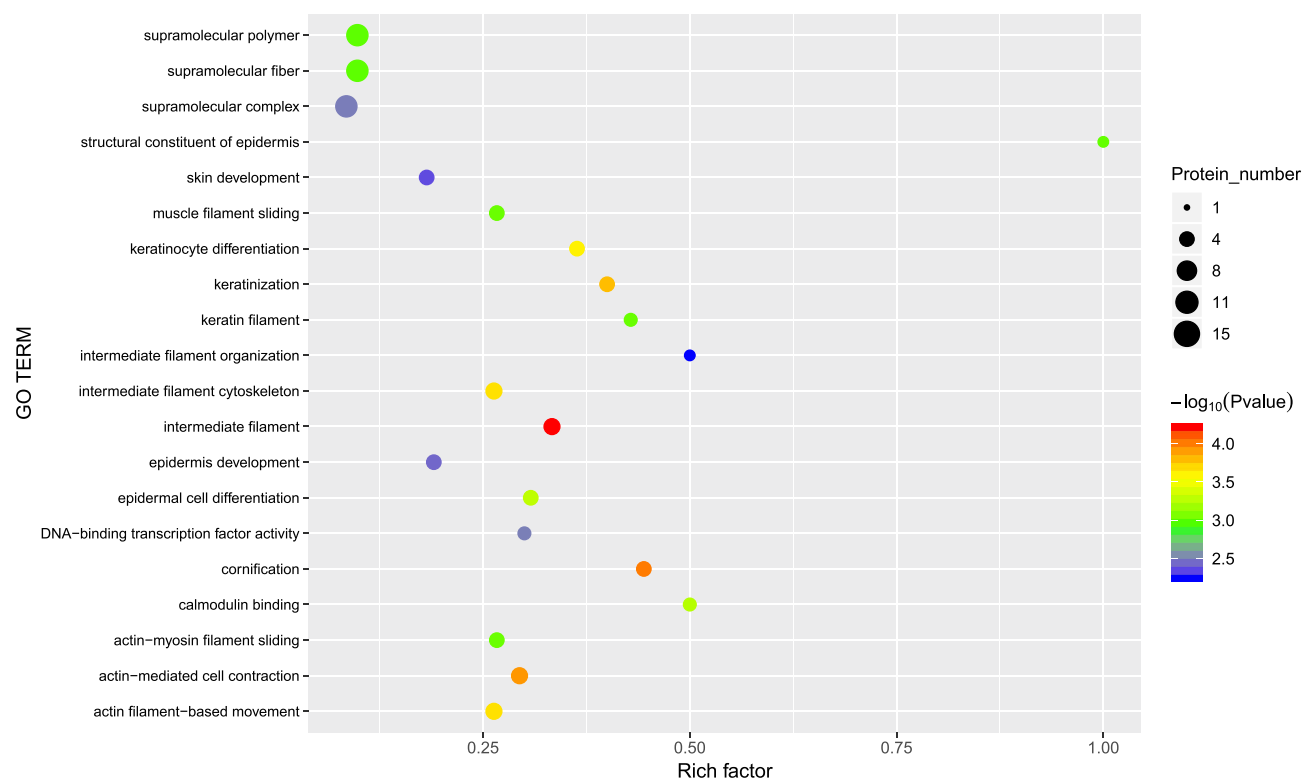
Figure 5 GO enrichment of functional terms. The size of the bubble represents the number of proteins with the GO classification. Fisher's exact test P value: the enrichment test P value was obtained using Fisher's exact test; −log10 (P value): logarithmically converted P value obtained with Fisher's exact test. The P value was not adjusted for the false discovery rate.

pathways were involved in EBV infection, salmonella infection, fluid shear stress, and AS. The five pathways associated with the downregulated DEPs were pathways in cancer, *Staphylococcus aureus* infection, the estrogen signaling pathway, the regulation of the actin cytoskeleton and focal adhesion (Figure 6). Our KEGG pathway enrichment analysis revealed that Epstein–Barr virus infection, viral myocarditis, colorectal cancer, nonalcoholic fatty liver disease (NAFLD) and amyotrophic lateral sclerosis (ALS) were the main pathways (Figure 7). Among the DEPs identified in the present study, those related to the five aforementioned pathways were CYCS, RAC1, PSMD14 and COPS4 (Figure 8).

CYCS, RAC1 and PSMD14 May Play Important Roles in IVDD

To further study whether CYCS, RAC1, PSMD14 and COPS4 were differentially expressed between the two groups, we determined the levels of related proteins by Western blot analysis. The results showed that the expression levels of CYCS, RAC1 and PSMD14 were increased in the severe group, whereas the expression level of COPS4 did not significantly differ (Figure 9).

Discussion

LBP is a common and clinical manifestation of a comorbidity, and studies have revealed that IVDD is closely related to the pathogenesis of LBP. However, the mechanism underlying IVDD has not been elucidated. For this reason, we combined TMT and LC–MS data to measure the differences in the number of chronically stimulated acetyl cholinergic neurotransmitters among chronically stimulated cholinergic neurotransmitters. We found 2042 proteins, and 70 of these proteins were DEPs (30 increased proteins and 40 decreased proteins). KEGG pathway enrichment analysis revealed that EBV infection, myocarditis, colorectal cancer, NAFLD and ALS are important pathways involved in IVDD pathogenesis. Among the DEG-encoded proteins, CYCS, RAC1, PSMD14, and COPS4 were related to the five aforementioned pathways.
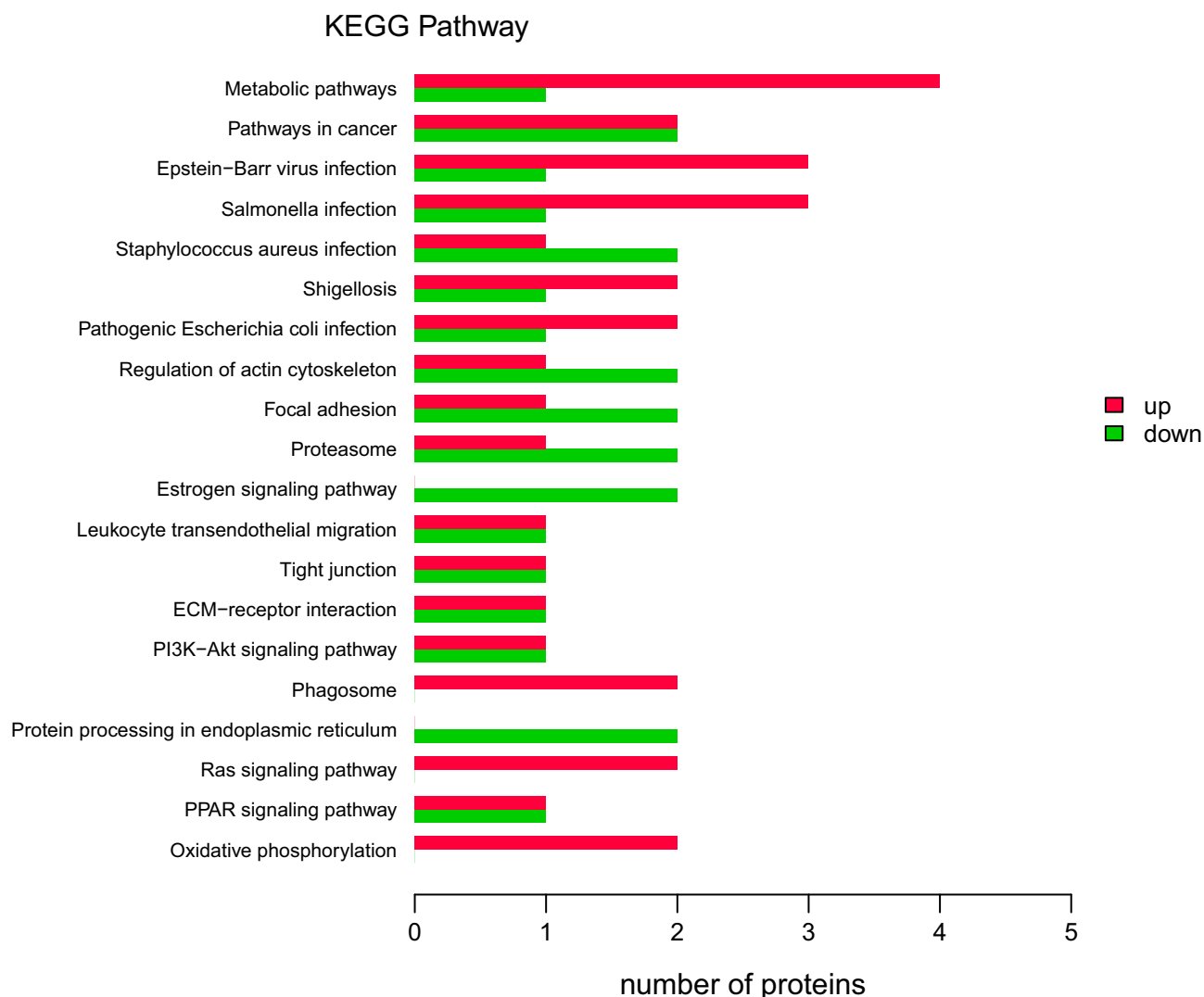
KEGG Pathway

Figure 6 KEGG pathway annotations of DEPs. The red bars indicate upregulated pathways, and the green bars indicate downregulated pathways.

CYCS, also known as cytochrome C, is an important molecule that widely exists in animals, plants and other organisms.[14] Under normal conditions, CYCS is located in mitochondria and is an important part of the electron transport chain. The dissociation of CYCS from mitochondria and its translocation to the cytoplasm are important events leading to apoptosis.[15] Guo et al reported that an increase in CYCS was positively correlated with lumbar disc degeneration, which was in line with our results.[16] In addition, the level of CYCS was also clearly increased in human degenerative NP samples in vitro.

Under normal circumstances, the lumbar disc is composed of NP with chondrocytes and a proteoglycan mucoid matrix. However, the accumulation of matrix fragments is a problem caused by aging: these matrix fragments increases proteoglycan depolymerization, gradually decrease the water content, thicken collagen and are gradually replaced by fibrocartilage.[17] Our data indicated that a nucleotide-binding protein, Ras-related C3 botulinum toxin substrate 1 (Rac1), was differentially increased in NP from the severe group. Rac1 promotes MMP-13 generation through fibronectin fragmentation. Consistently, active Rac1 has been detected in osteoarthritic cartilage.[18] In addition, there is evidence showing that Rac1 can increase the expression of ADAMTS-5 (ADAMTS-5), an enzyme used to dissolve cartilage proteoglycan aggregates that harbor the domain known as coagulation factor 1. We hypothesize that Rac1 plays a similar role in NP cells. Rac1 performs an essential
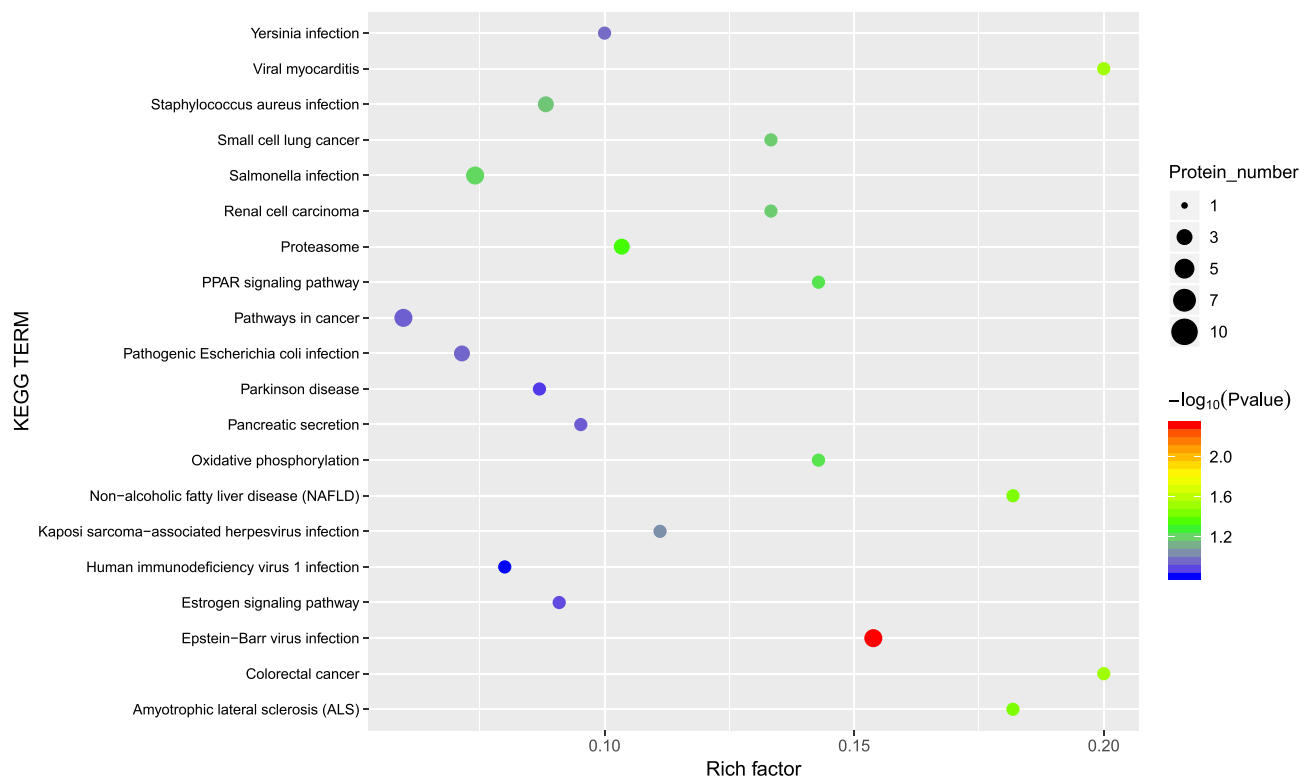
Figure 7 KEGG pathway enrichment of DEPs. The bubble size indicates the number of DEPs in the KEGG pathway. Fisher's exact test P value: enrichment P value obtained with Fisher's exact test; −log10 (P value): logarithmically converted P value obtained with Fisher's exact test. The P value was not adjusted for the false discovery rate.

function in the development of lumbar disc degeneration by facilitating chondrocyte and proteoglycan mucoid matrix destruction.

The proteasome is the key molecule that mediates protein hydrolysis. The proteasome system mainly includes a multifunctional protein complex (CP) called 19S RP (also known as PA700). The function of 19S RP is similar to that of an activator of the proteasome. The 19S RP level has been used to identify abnormally folded proteins because it is associated with the ubiquitination enzyme that forms K48 linkages. The results suggest that the LID subcomplex is a free subcomplex, suggesting that it has a biological function independent of 26S protein function, ie, it is part of an "abnormal signaling pathway". The most profound function of LID is deubiquitination mediated through the PSMD14/POH1/Rpn11 (hereinafter referred to as PSMD14) deubiquitination enzyme (DUB).[19] PSMD14 is an endogenous DUB subunit of the 26S proteasome and is located in the LID complex. The mechanism underlying the action of PSMD14 involves binding to a C-terminal isopeptide substrate to remove a polyubiquitin segment, thus promoting the transport of the substrate and degradation of the CP.[20] Although the proteasome system cannot degrade aggregated proteins, intriguingly, PSMD14 appears to exert a positive impact on autophagy function.[21] The cellular autophagy pathway is closely related to tumorigenesis, infection, neurodegenerative diseases and other diseases, whereas inhibition of cellular endocrine autophagy can delay the progression of these diseases.[22] Therefore, the upregulation of PSMD14 observed in the present study should be recognized and considered an important trait of the severe group.

COPS4 is a component of the COP9 signalosome and removes the ubiquitin-like protein Nedd8 to reduce the burden of misfolded proteins.[23] Additionally, the COP9 signalosome is related to obesity and is a significant risk factor for lumbar disc degeneration.

The lack of a disc source is the most important factor restricting basic research on IVDD. Related studies have shown that discs can be divided into five grades according to MRI. Normal discs are defined as Grade I or Grade II, whereas abnormal discs are defined as Grade III, Grade IV or Grade V. Considering the aforementioned
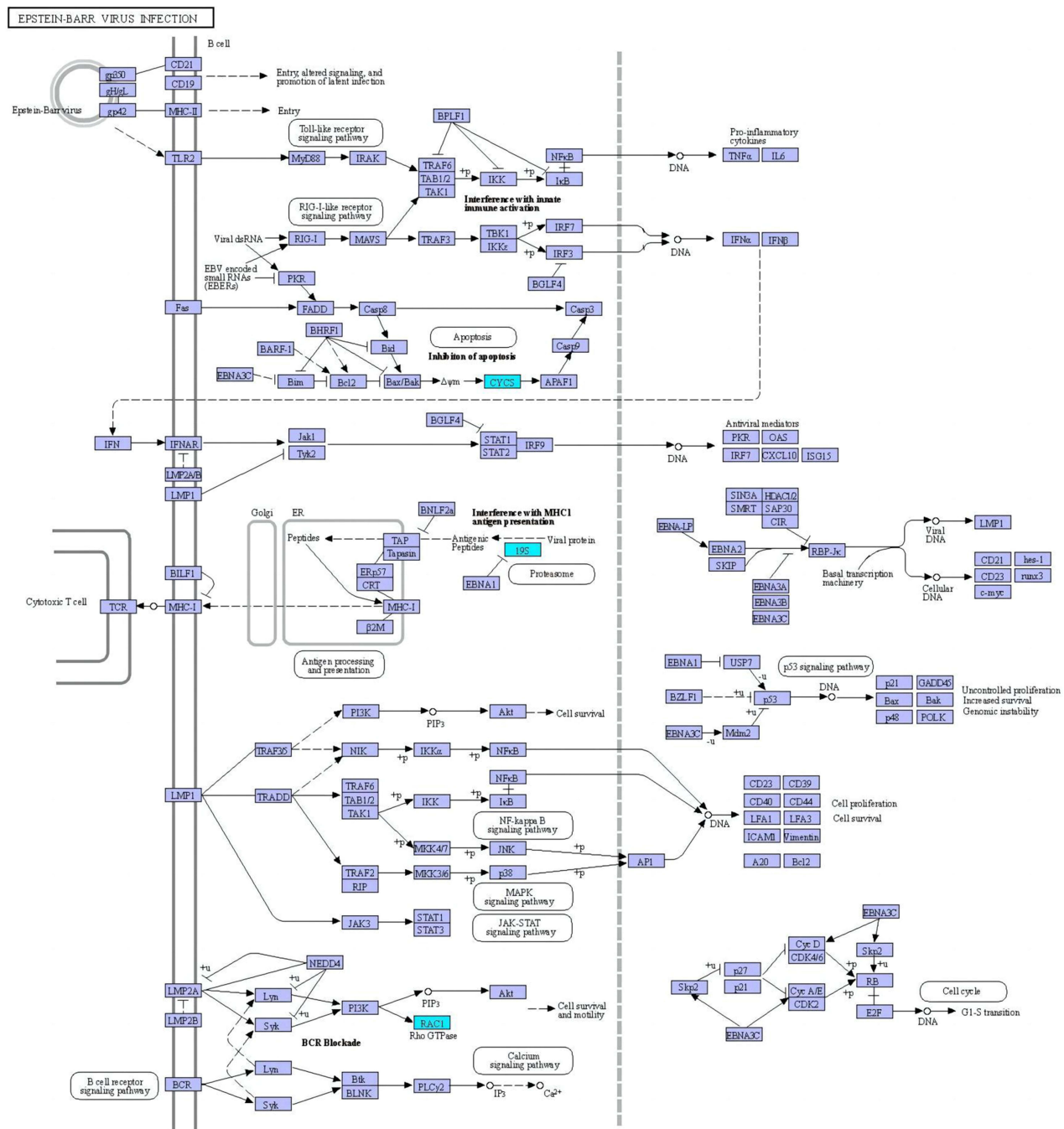
Figure 8 Epstein–Barr virus infection. The upregulated DEPs CYCS, 19S, and RAC1, which are highlighted in the blue frame, participate in Epstein–Barr virus infection.

limitations, the differential proteomic study of human NP cells in this project provides important clues for revealing the mechanism underlying the senescence and degeneration of NP cells. Due to the wide range of sample sources, the possible molecular targets identified in this study have theoretical importance and application value. In the future, this project will use the existing data to explore the molecular mechanism and clinical significance of IVDD.
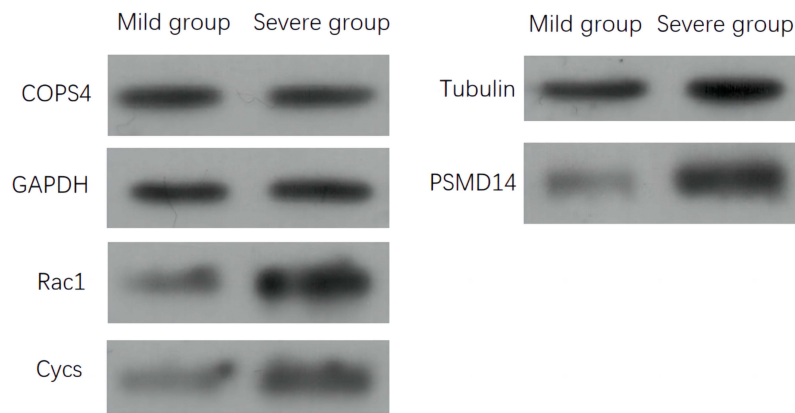
Figure 9 Analysis of the expression of related proteins in different groups. The CYCS, RAC1, PSMD14 and COPS4 levels were analyzed via Western blotting.

Conclusions

In this study, a comprehensive analysis of the DEPs in patients with intervertebral disc degeneration belonging to different age groups was conducted. This project lays the foundation for studying the pathogenesis of senile IVDD, especially the relationship between the immune inflammatory response in intervertebral discs and its involvement in IVDD. This study provides new ideas for the diagnosis and treatment of IVDD.

Data Sharing Statement

The datasets used and/or analyzed during the current study are available from the corresponding author upon reasonable request.

Ethics Approval and Consent to Participate

All treatments used in this study were performed according to relevant guidelines and rules, and informed consent was obtained from all the participants. The ethics committee of Zhejiang Hospital approved the study (Approval NO.:2022.156K). We followed the Declaration of Helsinki guidelines.

Acknowledgement

Author Contributions

All authors contributed to data analysis, drafting or revising the article, have agreed on the journal to which the article will be submitted, gave final approval of the version to be published, and agree to be accountable for all aspects of the work. Yang-Fu and Xiao-Qin Huang are co-first authors and contributed eqally to this article.

Funding

Disclosure

The authors declare that they have no competing interests in this work.

References

1. Bergknut N, Rutges JPHJ, Kranenburg H-JC, et al. The dog as an animal model for intervertebral disc degeneration? *Spine*. 2012;37(5):351–358. doi:10.1097/BRS.0b013e31821e5665
2. Fujii K, Yamazaki M, Kang JD, et al. Discogenic back pain: literature review of definition, diagnosis, and treatment. *JBMR Plus*. 2019;3(5):e10180. doi:10.1002/jbm4.10180

3. Kim KW, Chung H-N, Ha K-Y, et al. Senescence mechanisms of nucleus pulposus chondrocytes in human intervertebral discs. *Spine J*. 2009;9:658–666. doi:10.1016/j.spinee.2009.04.018

4. Rodrigues-Pinto R, Richardson SM, Hoyland JA, et al. Identification of novel nucleus pulposus markers: interspecies variations and implications for cell-based therapies for intervertebral disc degeneration. *Bone Joint Res*. 2013;2(8):169–178. doi:10.1302/2046-3758.28.2000184

5. Beack JY, Chun HJ, Bak KH, Choi KS, Bae IS, Kim KD. Risk factors of secondary lumbar discectomy of a herniated lumbar disc after lumbar discectomy. *J Korean Neurosurg Soc*. 2019;62(5):586–593. doi:10.3340/jkns.2019.0085

6. Chen X, Zhou QS, Xu L, et al. Does kyphotic configuration on upright lateral radiograph correlate with instability in patients with degenerative lumbar spondylolisthesis? *Clin Neurol Neurosurg*. 2018;173:96–100. doi:10.1016/j.clineuro.2018.07.020

7. Griffth J, Wang F, Antonio GE, et al. Modified pfirrmann grading system for lumbar intervertebral disc degeneration. *Spine J*. 2007;32(24):E708–E12. doi:10.1097/BRS.0b013e31815a59a0

8. Mesregah MK, Repajic M, Mgbam P, Fresquez Z, Wang JC, Buser Z. Trends and patterns of cervical degenerative disc disease: an analysis of magnetic resonance imaging of 1300 symptomatic patients. *Eur Spine J*. 2022;31(10):2675–2683. doi:10.1007/s00586-022-07336-2

9. Feng C, Yang M, Lan M, et al. ROS: crucial intermediators in the pathogenesis of intervertebral disc degeneration. *Oxid Med Cell Longev*. 2017;2017:5601593. doi:10.1155/2017/5601593

10. Hu J, Zhang Y, Jiang X, et al. ROS-mediated activation and mitochondrial translocation of CaMKII contributes to Drp1-dependent mitochondrial fission and apoptosis in triple-negative breast cancer cells by isorhamnetin and chloroquine. *J Exp Clin Cancer Res*. 2019;38(1):225. doi:10.1186/s13046-019-1201-4

11. Hartman R, Patil P, Tisherman R, et al. Age-dependent changes in intervertebral disc cell mitochondria and bioenergetics. *Eur Cell Mater*. 2018;36:171–183. doi:10.22203/eCM.v036a13

12. Rozanova S, Barkovits K, Nikolov M, Schmidt C, Urlaub H, Marcus K. Quantitative mass spectrometry-based proteomics: an overview. *Methods Mol Biol*. 2021;2228:85–116.

13. Kim YY, Um JH, Yoon JH, et al. p53 regulates mitochondrial dynamics by inhibiting Drp1 translocation into mitochondria during cellular senescence. *FASEB J*. 2020;34(2):2451–2464. doi:10.1096/fj.201901747RR

14. Santucci R, Sinibaldi F, Cozza P, Polticelli F, Fiorucci L. Cytochrome c: an extreme multifunctional protein with a key role in cell fate. *Int J Biol Macromol*. 2019;136:1237–1246. doi:10.1016/j.ijbiomac.2019.06.180

15. Zhang M, Zheng J, Nussinov R, Ma B. Release of cytochrome C from bax pores at the mitochondrial membrane. *Sci Rep*. 2017;7(1):2635. doi:10.1038/s41598-017-02825-7

16. Guo S, Su Q, Wen J, et al. S100A9 induces nucleus pulposus cell degeneration through activation of the NF-kappaB signaling pathway. *J Cell Mol Med*. 2021;25(10):4709–4720. doi:10.1111/jcmm.16424

17. Zhao K, An R, Xiang Q, et al. Acid-sensing ion channels regulate nucleus pulposus cell inflammation and pyroptosis via the NLRP3 inflammasome in intervertebral disc degeneration. *Cell Proliferation*. 2021;54(1):e12941. doi:10.1111/cpr.12941

18. Marei H, Malliri A. Rac1 in human diseases: the therapeutic potential of targeting Rac1 signaling regulatory mechanisms. *Small GTPases*. 2017;8(3):139–163. doi:10.1080/21541248.2016.1211398

19. Bustamante HA, Albornoz N, Morselli E, Soza A, Burgos PV. Novel insights into the non-canonical roles of PSMD14/POH1/Rpn11 in proteostasis and in the modulation of cancer progression. *Cell Signal*. 2023;101:110490. doi:10.1016/j.cellsig.2022.110490

20. Gong Y, Wei ZR. Identification of PSMD14 as a potential novel prognosis biomarker and therapeutic target for osteosarcoma. *Cancer Rep*. 2022;5(7):e1522. doi:10.1002/cnr2.1522

21. Sun T, Liu Z, Bi F, Yang Q. Deubiquitinase PSMD14 promotes ovarian cancer progression by decreasing enzymatic activity of PKM2. *Mol Oncol*. 2021;15(12):3639–3658. doi:10.1002/1878-0261.13076

22. Zheng Q, Shen H, Tong Z, et al. A thermosensitive, reactive oxygen species-responsive, MR409-encapsulated hydrogel ameliorates disc degeneration in rats by inhibiting the secretory autophagy pathway. *Theranostics*. 2021;11(1):147–163. doi:10.7150/thno.47723

23. Lee T, Lee H. Shared blood transcriptomic signatures between alzheimer's disease and diabetes mellitus. *Biomedicines*. 2021;9(1):1.